Sustained High-Frequency Dynamic Instability of a Nonlinear System of Coupled Oscillators Forced by Single or Repeated Impulses: Theoretical and Experimental Results

Kevin Remick[1]
e-mail: remick2@illinois.edu

Alexander Vakakis

Department of Mechanical Science and Engineering, University of Illinois at Urbana-Champaign, 1206 W. Green Street, Urbana, IL 61801

Lawrence Bergman

D. Michael McFarland

Department of Aerospace Engineering, University of Illinois at Urbana-Champaign, 104 S. Wright Street, Urbana, IL 61801

D. Dane Quinn
Department of Mechanical Engineering, University of Akron, Akron, OH 44325

Themistoklis P. Sapsis
Department of Mechanical Engineering, Massachusetts Institute of Technology, Cambridge, MA 02139

This report describes the impulsive dynamics of a system of two coupled oscillators with essential (nonlinearizable) stiffness nonlinearity. The system considered consists of a grounded weakly damped linear oscillator coupled to a lightweight weakly damped oscillating attachment with essential cubic stiffness nonlinearity arising purely from geometry and kinematics. It has been found that under specific impulse excitations the transient damped dynamics of this system tracks a high-frequency impulsive orbit manifold (IOM) in the frequency-energy plane. The IOM extends over finite frequency and energy ranges, consisting of a countable infinity of periodic orbits and an uncountable infinity of quasi-periodic orbits of the underlying Hamiltonian system and being initially at rest and subjected to an impulsive force on the linear oscillator. The damped nonresonant dynamics tracking the IOM then resembles continuous resonance scattering; in effect, quickly transitioning between multiple resonance captures over finite frequency and energy ranges. Dynamic instability arises at bifurcation points along this damped transition, causing bursts in the response of the nonlinear light oscillator, which resemble self-excited resonances. It is shown that for an appropriate parameter design the system remains in a state of sustained high-frequency dynamic instability under the action of repeated impulses. In turn, this sustained instability results in strong energy transfers from the directly excited oscillator to the lightweight nonlinear attachment; a feature that can be employed in energy harvesting applications. The theoretical predictions are confirmed by experimental results. [DOI: 10.1115/1.4025605]

Keywords: dynamical instability, strong nonlinearity, impulsive excitation

1 Introduction

It has been shown that linear damped oscillators with essentially nonlinear damped attachments provide a means for efficient broadband vibration suppression [1–3], in contrast to the linear vibration absorber whose operation is narrowband [4]. Targeted energy transfer has been observed in these strongly nonlinear systems, with the attachments being commonly referred to as nonlinear energy sinks [5,6]. Targeted energy transfer describes the nearly irreversible passive transfer of a significant amount of energy initially stored in a linear structure to an appropriately designed strongly nonlinear lightweight attachment which acts, in essence, as a passive broadband adaptive boundary controller [7–12]. The complex dynamics of these systems results from the capacity of the essentially nonlinear attachment to engage in resonance captures with modes of the linear structure over an extensive range of frequencies and energies. This behavior arises from the dynamics of the underlying Hamiltonian systems, which possess highly degenerate eigenstructures with pairs of complex conjugate imaginary and multiple zero eigenvalues. These result in complex high codimensional bifurcations, which may lead to interesting nonlinear dynamics such as chaotic motions and dynamic instabilities.

An additional interesting feature of this class of highly degenerate systems is the occurrence of nonlinear instabilities associated with geometric stiffness [13] or damping nonlinearities [3]. In Ref. [3] a rather unexpected result was reported; namely, that a geometrically nonlinear viscous damping element can lead to dynamical instability of the linear oscillator to which it is attached. This instability appeared as a buildup of the response of a nonlinear attachment as it engaged in resonance capture with the linear oscillator, in similarity to classical self-excited systems with energy intake such as the Van der Pol oscillator or systems undergoing aeroelastic flutter. An additional interesting dynamical phenomenon reported in Ref. [13], where a peculiar damped nonlinear transition into a state of sustained nonlinear resonance scattering [14–16] in a system of two coupled oscillators with essential stiffness was reported. This transition was realized only for sufficiently weak damping and only in the neighborhood of the low-frequency branch of the impulsive orbit manifold (IOM) of the underlying Hamiltonian dynamical system. Moreover, sustained resonance scattering was realized only in certain frequency ranges and was eliminated when the dynamics was attracted to a 1:3 resonance capture which was manifested as dynamic instability in the transient response of the system, in a manner similar to that in Ref. [3].

In a Hamiltonian system of coupled oscillators with strong stiffness nonlinearities, an IOM consists of a countable infinity of

[1]Corresponding author.

Contributed by the Design Engineering Division of ASME for publication in the JOURNAL OF VIBRATION AND ACOUSTICS. Manuscript received March 1, 2013; final manuscript received September 18, 2013; published online November 13, 2013. Assoc. Editor: Philip Bayly.

periodic orbits and an uncountable infinity of quasi-periodic orbits and typically extends over broad frequency and energy ranges [17]. These orbits, which are in the form of nonlinear beats, arise when an impulsive force is applied to the linear oscillator with the system being initially at rest. A periodic impulsive orbit corresponds to a rational relationship of the dominant frequencies of the responses of the oscillators, while a quasi-periodic impulsive orbit corresponds to an irrational frequency relationship. As shown in Refs. [3,13] and in the present work, dynamic instability is associated with excitation of the dynamics in the neighborhood of the IOM.

The present work extends the aforementioned results in two ways. First, it is shown that sustained high-frequency dynamical instability can be realized in systems of impulsively excited strongly nonlinear coupled oscillators; this contrasts with previously reported results [3,13], where only low-frequency dynamic instabilities were reported. Second; in contrast to previous studies where free damped transitions were considered, the nonlinear dynamics under a repetitive series of impulses are considered in this report and it is shown that the dynamic instability can be sustained under this type of periodic excitation. It is anticipated that these findings will find application in areas such as energy harvesting of vibrations of systems under periodic or near-periodic excitations. These theoretical findings are validated by a series of experimental tests.

2 System Configuration and Impulsive Forcing Scenarios

The configuration of the system of coupled oscillators is depicted in Fig. 1. It is composed of a grounded weakly damped linear oscillator coupled to a lightweight attachment through a linear weak viscous damper and an essentially nonlinear spring of the third order (i.e., possessing cubic nonlinearity and no linear stiffness component). Geometric and kinematic nonlinearities in this system are realized due to transverse deformations of the linear springs with constants k_3 relative to the direction of oscillation of the attachment [12]. An excitation $f(t)$ is applied to the linear oscillator at $t=0$ with the system at rest.

The equations of motion of the system shown in Fig. 1 are expressed in normalized form as follows:

$$\ddot{x} + \lambda_1\dot{x} + \lambda_2(\dot{x}-\dot{\nu}) + \omega_0^2 x + C(x-\nu)^3 = F(t) \tag{1a}$$

$$\varepsilon\ddot{\nu} + \lambda_2(\dot{\nu}-\dot{x}) + C(\nu-x)^3 = 0 \tag{1b}$$

where x denotes the response of the linear oscillator, v is the response of the nonlinear oscillator, and the over-dot denotes differentiation with respect to the time variable t. The normalized parameters are defined as $\omega_0=(k_1/m_1)^{1/2}$, $C=k_3/m_1$, $\lambda_1=b_1/m_1$, $\lambda_2=b_2/m_1$, $\varepsilon=m_2/m_1$, and $F(t)=f(t)/m_1$, where the physical parameters are presented in Fig. 1. By considering the small mass parameter $0<\varepsilon\ll 1$, the lightweightness of the nonlinear attachment compared to the directly excited linear oscillator is denoted. This work considers impulsive forcing excitation in the form of single or repetitive impulses.

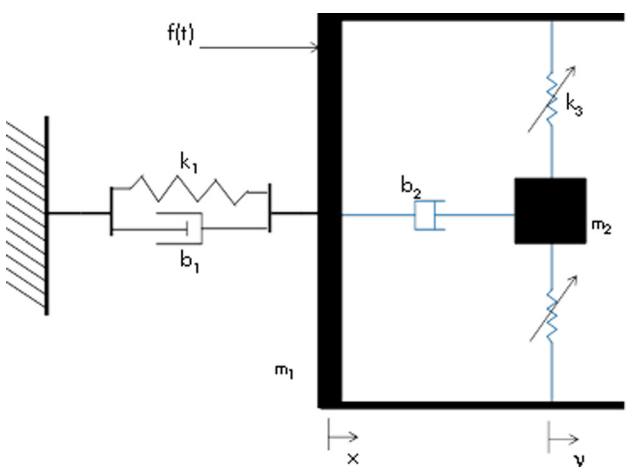

Fig. 1 Configuration of the two-degree-of-freedom coupled oscillator with essential geometric nonlinearity

The first excitation scenario of a single impulse was studied by Anderson et al. [13] and it was shown, both theoretically and experimentally, that the corresponding damped transition approximately tracks the lower frequency branch of the impulsive orbit manifold(IOM) of the underlying Hamiltonian system (that is, system (1) with the damping constants set equal to zero). This work will generalize these results by showing the high-frequency IOM tracking by the damped dynamics of system (1). In turn, these high-frequency dynamics will be manifested as the dynamic instability of the coupled system in the form of relatively high-amplitude and high-frequency oscillations of the (indirectly forced) nonlinear attachment. Moreover, in the single impulse excitation scenario it is assumed that system (1) is initially at rest at $t=0-$, and a single impulse equal to $F(t)=I_0\delta(t)$ is applied to the linear oscillator at $t=0+$. Hence, the equations of motion (1) are complemented by the initial conditions

$$x(0+)=0, \quad \dot{x}(0+)=I_0, \quad v(0+)=\dot{v}(0+)=0 \tag{2}$$

In the second excitation scenario, the linear oscillator is excited by a periodic series of identical impulses. For the first impulse, it is assumed again that at $t=0-$ the system is initially at rest, therefore, immediately after the initial impulse is applied the initial conditions are given by Eq. (2). This case defines the impulsive period T as the time delay between consecutive impulses and the normalized impulsive period as the multiple n of the fundamental period $T_0=2\pi/\omega_0$ of the linear oscillator between consecutive impulses, $n=T/T_0$. For example, a normalized impulsive period of 5 would define a periodic forcing scheme in which an impulse of magnitude I_0 is applied to the linear oscillator every five fundamental periods. In mathematical form the periodic series of impulses is defined as $F(t;T)=\sum_{k=0}^{N} I_0\,\delta(t-kT)$, where N denotes the total number of applied impulses in the given computation or experiment. In this scheme, the pth impulse applied to the linear oscillator at $t=pT+$, $p\geq 1$ corresponds to the following initial conditions for system (1) immediately after the application of the pth impulse:

$$\begin{aligned} &x(pT+)=x(pT-), \quad \dot{x}(pT+)=\dot{x}(pT-)+I_0, \\ &v(pT+)=v(pT-), \quad \dot{v}(pT+)=\dot{v}(pT-), \quad p=1,\ldots,N \end{aligned} \tag{3}$$

Hence, the initial state of the system will differ for each consecutive impulse, depending on the remaining vibration energy in the two coupled oscillators at the time of application of the pth impulse. In Eq. (3), continuity for all state variables at the time of application of the impulse is imposed, except for the velocity of the linear oscillator, which exhibits a discontinuity equal to the intensity of the applied impulse.

Various impact periods and impulse magnitudes are considered to study the occurrence of sustained dynamic instability in this system, manifested as the repetitive excitation of high-frequency and relatively high-amplitude oscillations of the (indirectly forced) lightweight attachment in the neighborhood of a high-frequency part of the IOM of the underlying Hamiltonian system. Since the dynamics of the corresponding undamped system (1) play an important role in exciting sustained dynamic instability in this system, Sec. 3 is devoted to a brief overview of the underlying Hamiltonian dynamics and discusses the IOM of this system.

3 Underlying Hamiltonian Dynamics

Before studying the dynamics of system (1), the underlying Hamiltonian system corresponding to $\lambda_1=\lambda_2=F(t)=0$ is

considered by depicting its dynamics in a frequency energy plot (FEP) [2,12,13]. This plot depicts branches of periodic and quasi-periodic orbits at varying energy levels. In particular, the dominant frequency of each orbit is plotted as a function of the (conserved) energy. The Hamiltonian FEP will be used as a framework to study the forced dynamics of the weakly damped system (1) since, depending on the applied initial energy, the weakly damped dynamics will transition between different branches of the FEP; this will be shown by computing the wavelet transform spectra of the damped responses and superimposing these spectra on the Hamiltonian FEP. The wavelet transform will be applied in order to analyze a time series of a given transient response to obtain frequency transitions as wavelet spectra. The wavelet transform involves a windowing technique with variable-sized regions, in which small time intervals are considered for high-frequency components and, conversely, larger time intervals are considered for lower frequency components. This provides a valuable 'dynamic' time-frequency analysis tool, which is more beneficial compared to the stationary signal analysis provided by the fast Fourier transform in the sense that it reveals the temporal evolutions of the dominant frequency components of a given damped transition as energy decreases due to damping dissipation. Depending on the level of damping and the initial state of the system, this damped transition will be shown to 'visit' and make transitions between different branches of the FEP with decreasing energy.

In Fig. 2 the FEP of the underlying Hamiltonian system (1) for the parameters

$$\varepsilon = 8.814 \times 10^{-2}, \quad \omega_0 = 15.367 \text{ rad/s}, \quad C = 4.315 \times 10^6 \text{ N/Kgm}^3$$

is presented; these parameters correspond approximately (with the exception of the exponent of the essential stiffness nonlinearity as discussed in the following text) to the experimental system that will be considered in a following section with un-normalized parameters

$$m_1 = 1.9853 \text{ Kg}, m_2 = 0.175 \text{ Kg}, \quad k_1 = 469 \text{ N/m}, \quad k_3 = 8.568 \times 10^6 \text{ N/m}^3$$

Two *global backbone branches* of orbits are presented which are defined over broad frequency and energy ranges; namely, branches $S11\pm$ corresponding to in-phase and out-of-phase periodic orbits in 1:1 resonance, with both oscillators of the system vibrating with identical frequencies. Two of the countable infinity of *local subharmonic tongues* are also depicted; namely, branches

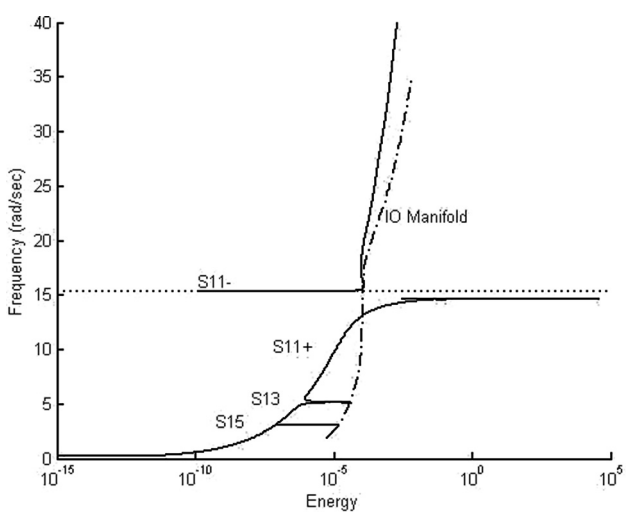

Fig. 2 Frequency-energy plot of the underlying Hamiltonian system (1)

$S13$ and $S15$ corresponding to 1:3 and 1:5 resonances, respectively, between the linear oscillator and the nonlinear attachment (which oscillates with lower frequency). As discussed in Ref. [12], the countable infinity of periodic orbits lie on pairs of in-phase/out-of-phase subharmonic tongues (such as the depicted branches $S13$ and $S15$), which are defined over finite energy ranges and are connected to the backbone branches (in fact, each of these subharmonic tongues represents mode mixing between the in-phase and out-of-phase modes of the system).

Of particular interest to this study will be the impulsive orbit manifold (IOM) of the Hamiltonian system. The IOM consists of a countable infinity of periodic orbits and an uncountable infinity of quasi-periodic orbits of the Hamiltonian system corresponding to the initial impulsive excitation of the linear oscillator and all other initial conditions zero; i.e., $\dot{x}(0+) = I_0$, $x(0+) = v(0+) = \dot{v}(0+) = 0$. In Ref. [13], it was shown, analytically and experimentally, that damped transitions in the neighborhood of the low-frequency portion of the IOM imply sustained nonlinear resonance scattering on that manifold. That work predicted that damping plays a critical role in exciting this type of damped transitions (i.e., 'tracking' the IOM); specifically, light damping allows for a slow variation of energy in the system, leading to sustained resonance scattering away from basins of attraction to resonance captures. Indeed, increased damping causes the breakdown of resonance scattering, which results in immediate resonance capture. As shown in Sec. 4, under single or repetitive impulsive excitation of the linear oscillator in the damped system (1), the resulting dynamical transitions in neighborhoods of the high-frequency portion of the IOM will be responsible for sustained instability of the dynamics, appearing as multifrequency high-amplitude oscillations of the nonlinear attachment.

The superposition of the wavelet spectrum of a specific damped transient response on the Hamiltonian FEP of Fig. 2 provides valuable qualitative and quantitative information regarding the frequency content of the damped dynamics. Although such FEP-wavelet superpositions are purely phenomenological, one needs to consider that the dynamical effects of weak viscous damping are purely parasitic, i.e., they do not introduce any new dynamics in the system compared to the underlying Hamiltonian one. Hence, the FEP depictions of the wavelet spectra of the damped transitions provide information on the branches of solutions of the underlying Hamiltonian system that are 'visited' in a given damped transition; the actual transitions between branches are then dictated by the level and distribution of damping within the system. For more information of the use of the FEP to study transient nonlinear dynamics the reader is referred to Ref. [12] and the references therein. To construct the FEP depictions in the results of the following sections, one applies the following sequence of computations: (i) for a given impulse (or series of impulses) applied to the linear oscillator one computes the numerical wavelet spectrum of the responses of the system, (ii) at any given time, one computes the total (continuously decreasing) instantaneous energy of the system following the application of the impulse, and (iii) by plotting the frequency responses obtained by the wavelet spectra versus the corresponding instantaneous energy (i.e., eliminating the time variable) one obtains a frequency-energy depiction of the damped transition, which can be superimposed to the Hamiltonian FEP in order to study the nonlinear dynamic transitions that occur in the dynamics.

Section 4 initiates the study of the damped dynamics of system (1) by performing numerical simulations for single and repetitive impulse excitation, and studies the resulting high-frequency dynamical instabilities by wavelet analysis and superpositions of the wavelet spectra on the FEP of Fig. 2. The two impulse excitation scenarios are separately considered.

4 Computational Study

The computational study of the damped dynamics of Eq. (1) is initiated by considering single impulse excitation and studying the

Table 1 Physical system parameters for the model of Fig. 1

Parameter	Value
m_1	1.9853 Kg
m_2	0.175 Kg
k_1	469 N/m
k_3	25.068×10^6 N/m^3
b_1	0.0726 N s/m
b_2	0.0030 N s/m

Table 2 Normalized parameters for the model of Fig. 1

Parameter	Value
ε	8.814×10^{-2}
ω_0	15.367 rad/s
C	12.627×10^6 N/Kg m^3
λ_1	0.0366 N s/Kg m
λ_2	0.00151 N s/Kg m

resulting damped transitions by superimposing their wavelet spectra on the FEP of the underlying Hamiltonian system. Although this type of superposition is purely phenomenological, it will help one interpret the damped response in terms of resonance captures or resonance scattering in the branches of the FEP visited during that specific response [12]. The system parameters for the model of Fig. 1 were selected as shown in Table 1, which correspond to the normalized parameters for the theoretical model (1) shown in Table 2. These parameters differ from the experimentally identified parameters for the experimental model discussed in Sec. 5, the reason being that no linear component complementing the nonlinear stiffness was considered so that the nonlinear coefficient k_3 had to be adjusted to account for its purely (essentially) nonlinear nature. In addition, purely cubic stiffness nonlinearity was assumed in this theoretical model, in contrast to the experimentally estimated nonlinear exponent of 2.95 as discussed in Sec. 5. All frequency-energy Hamiltonian plots utilized in this section were computed using the previous adjusted system parameters.

Here, note that in the preceding theoretical model there is a great reduction of the mass ratio ε compared to the system considered by Anderson et al. [13] with a mass ratio of $\varepsilon = 0.4046$; as shown in the following text, this drastic reduction of the mass of the nonlinear attachment has a drastic effect on the damped dynamics and, in particular, its frequency content. In particular, whereas in Ref. [13] it was shown that the dynamics can track the lower frequency portion of the IOM, in the present case with the much lighter nonlinear attachment, the dynamics will be shown to track the higher frequency portion of the IOM, resulting in high-frequency dynamic instability of the system.

The theoretical model (1) was numerically integrated with the initial conditions (2) for a range of applied impulses in order to study the effect of the energy input on the damped dynamics. Figure 3 depicts the response of the theoretical model subject to a single impulse of relatively small intensity $I_0 = 0.007$ m/s. Although the responses of the linear oscillator and the nonlinear attachment are small, interesting resonance captures in the damped dynamics are observed when considering the wavelet spectrum of the relative response $x - v$ (cf., Fig. 3(*c*)) and superimposing it on the FEP of the underlying Hamiltonian system (cf., Fig. 3(*d*)). It is deduced that the dynamics initially engages in resonance capture in the vicinity of the $S11-$ out-of-phase backbone branch before transitioning to the lower frequency $S13$ subharmonic tongue, which results in a gradually increasing (albeit small) amplitude of oscillation of the nonlinear attachment. This type of low-frequency damped transition is typical of transitions reported in previous works [12,13] and the corresponding dynamical instabilities reported therein. In this case, the initial energy input into the system provided by the impulse is too low to cause high-frequency transient dynamic instability associated with tracking of the high-frequency portion of the IOM.

The response of the system for the normalized impulse intensity of $I_0 = 0.010$ m/s is shown in Fig. 4. It is clear that a small increase in the input energy results in a qualitatively different dynamic response. In particular, in the initial highly energetic regime the response of the nonlinear attachment occurs in the neighborhood

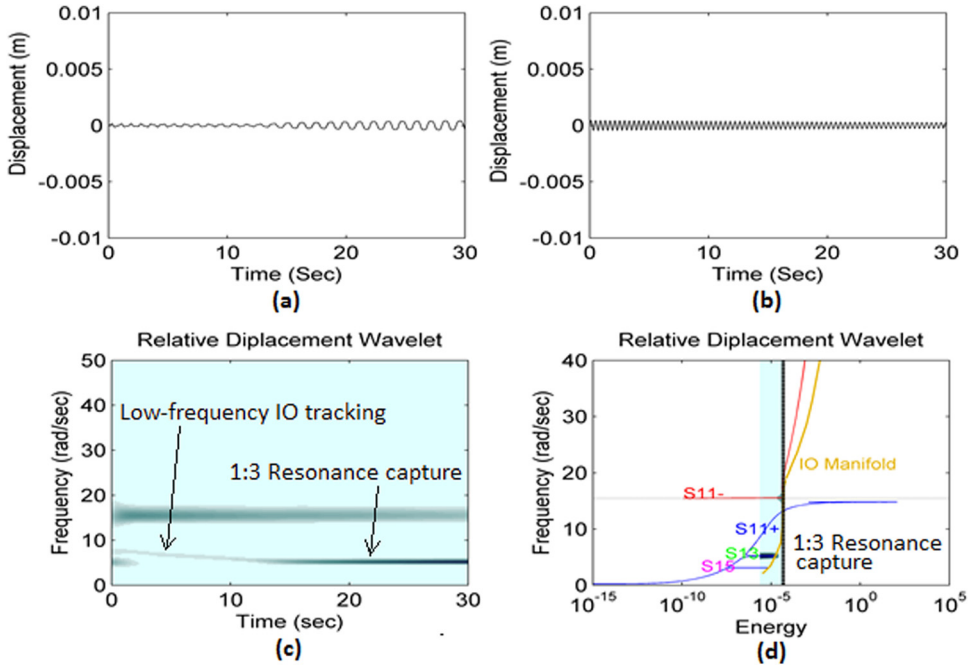

Fig. 3 Damped response of the theoretical model for single impulse excitation of normalized intensity $I_0 = 0.007$ m/s: (*a*) displacement of the nonlinear attachment, (*b*) displacement of the linear oscillator, (*c*) wavelet spectrum of the relative displacement, and (*d*) wavelet spectrum of (*c*) superimposed on the Hamiltonian FEP

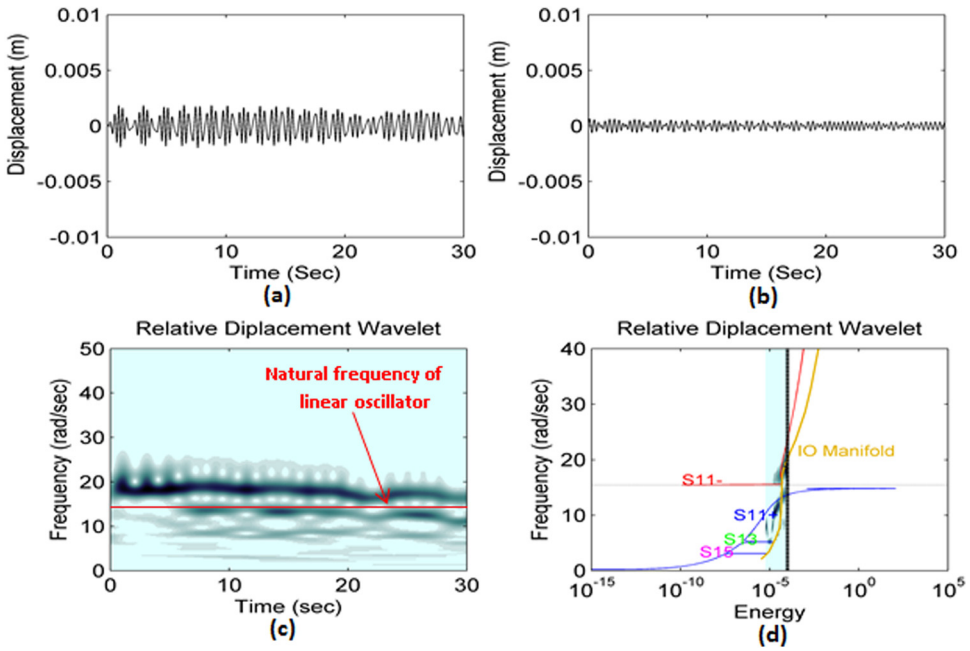

Fig. 4 Damped response of the theoretical model for single impulse excitation of normalized intensity $I_0 = 0.010$ m/s: (*a*) displacement of the nonlinear attachment, (*b*) displacement of the linear oscillator, (*c*) wavelet spectrum of the relative displacement, and (*d*) wavelet spectrum of (*c*) superimposed on the Hamiltonian FEP

of the intersection between the out-of-phase backbone branch $S11-$ and the high-frequency portion of the IOM; this is deduced by the strong high-frequency harmonics in the initial part of the wavelet spectrum of the damped relative response of Fig. 4(*c*). In the later part of the damped responses, broadband beat phenomena (appearing as pulsations) in the wavelet spectrum of Fig. 4(*c*) are noted; these nonlinear beats result due to the existence of closely spaced resonance captures as the IOM approaches the out-of-phase $S11-$ branch [17]. These phenomena result in the high-frequency dynamical instability in the damped response, which manifests itself in the form of strongly modulated damped responses of both the linear oscillator and (especially) the nonlinear attachment. It is important to note again that this dynamic instability arises from the presence of the essential stiffness nonlinearity and weak viscous damping in the coupling, since it cannot be realized in linear or weakly nonlinear settings. Moreover, to the authors' best knowledge, this is the first report of *high-frequency dynamical instability* by tracking of the high-frequency

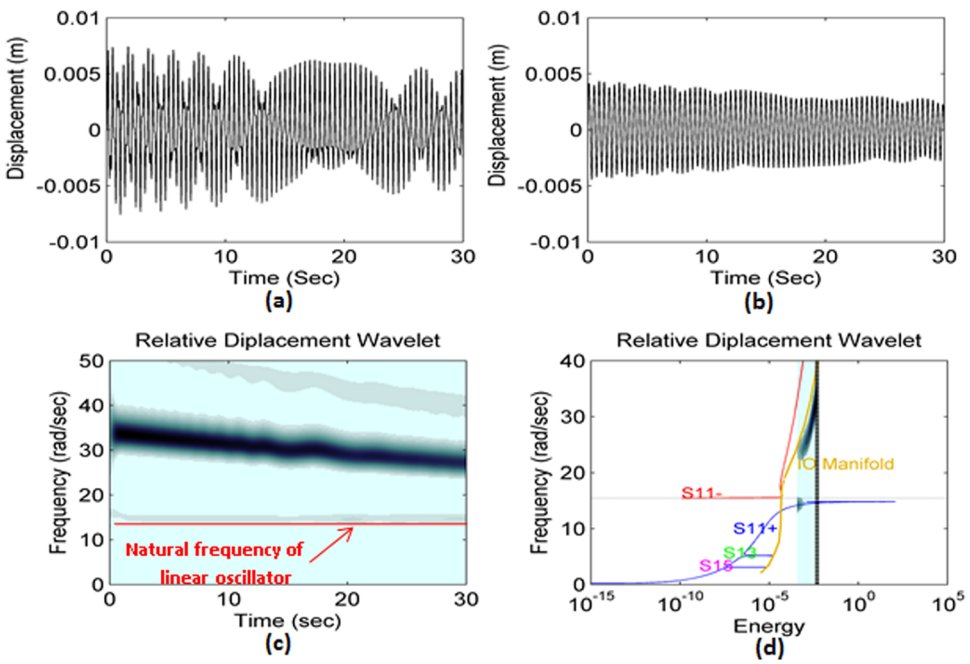

Fig. 5 Damped response of the theoretical model for single impulse excitation of normalized intensity $I_0 = 0.070$ m/s: (*a*) displacement of the nonlinear attachment, (*b*) displacement of the linear oscillator, (*c*) wavelet spectrum of the relative displacement, and (*d*) wavelet spectrum of (*c*) superimposed on the Hamiltonian FEP

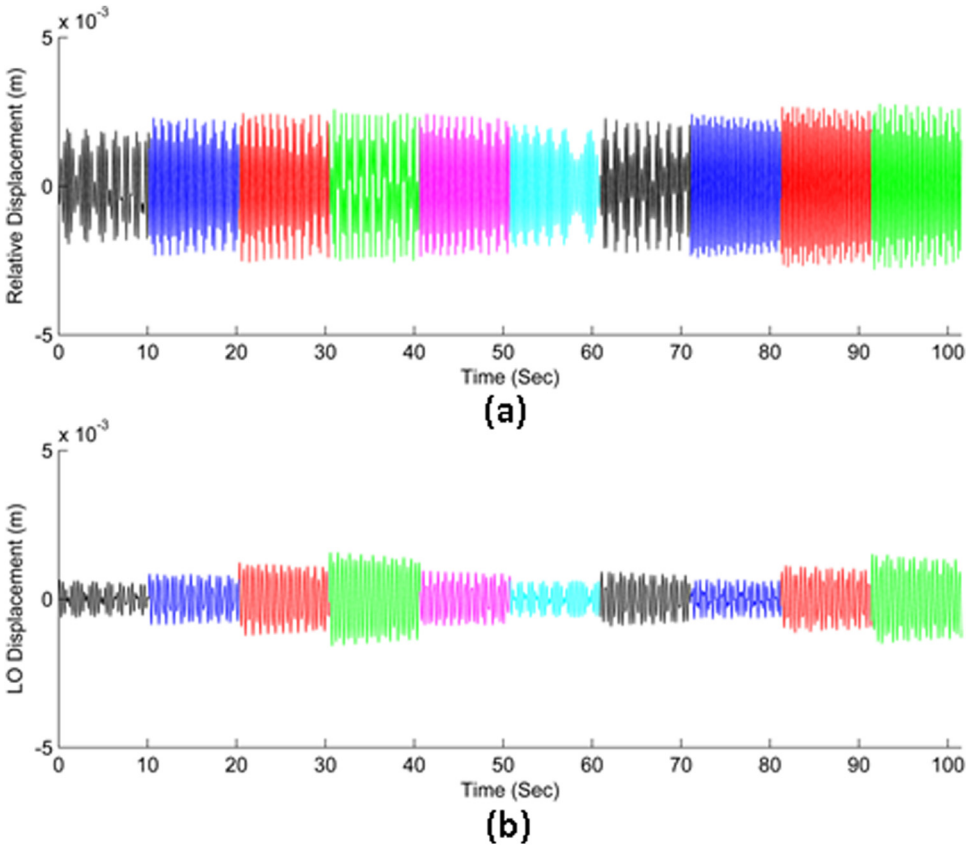

Fig. 6 Damped response of the theoretical model for periodic impulse excitation of normalized intensity $I_0 = 0.010$ m/s: (*a*) relative displacement between the nonlinear attachment and the linear oscillator, and (*b*) displacement of the linear oscillator

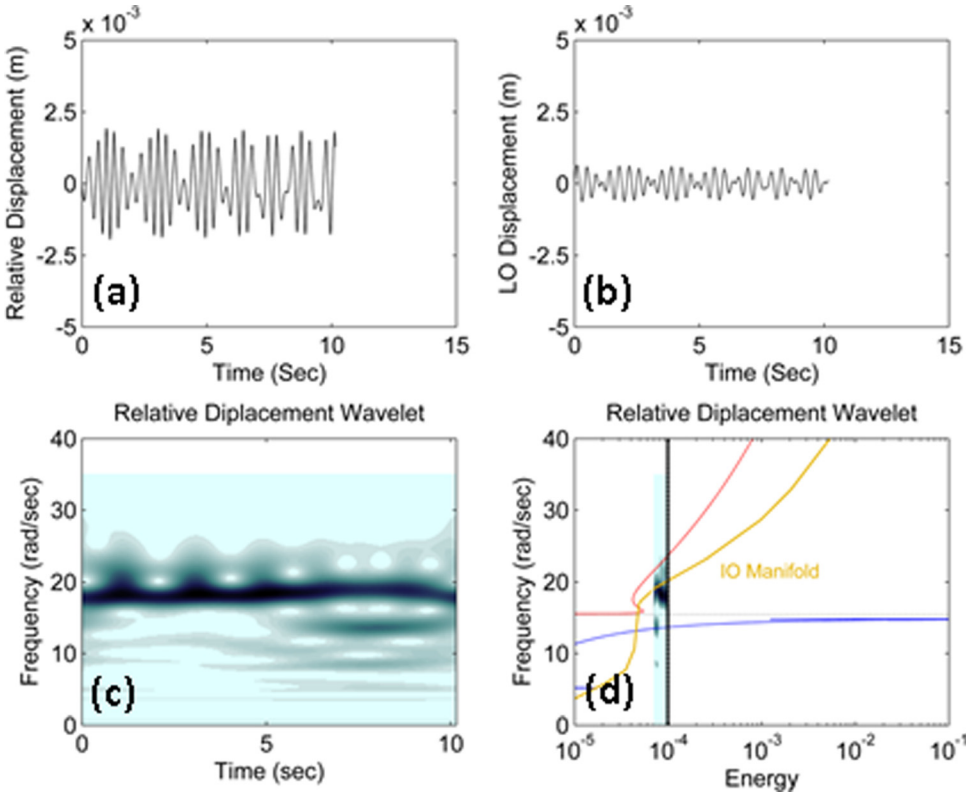

Fig. 7 First cycle of the damped response of Fig. 6, following the first impulse: (*a*) relative displacement between the nonlinear attachment and the linear oscillator, (*b*) displacement of the linear oscillator, (*c*) wavelet spectrum of the relative displacement, and (*d*) wavelet spectrum of (*c*) on the Hamiltonian FEP

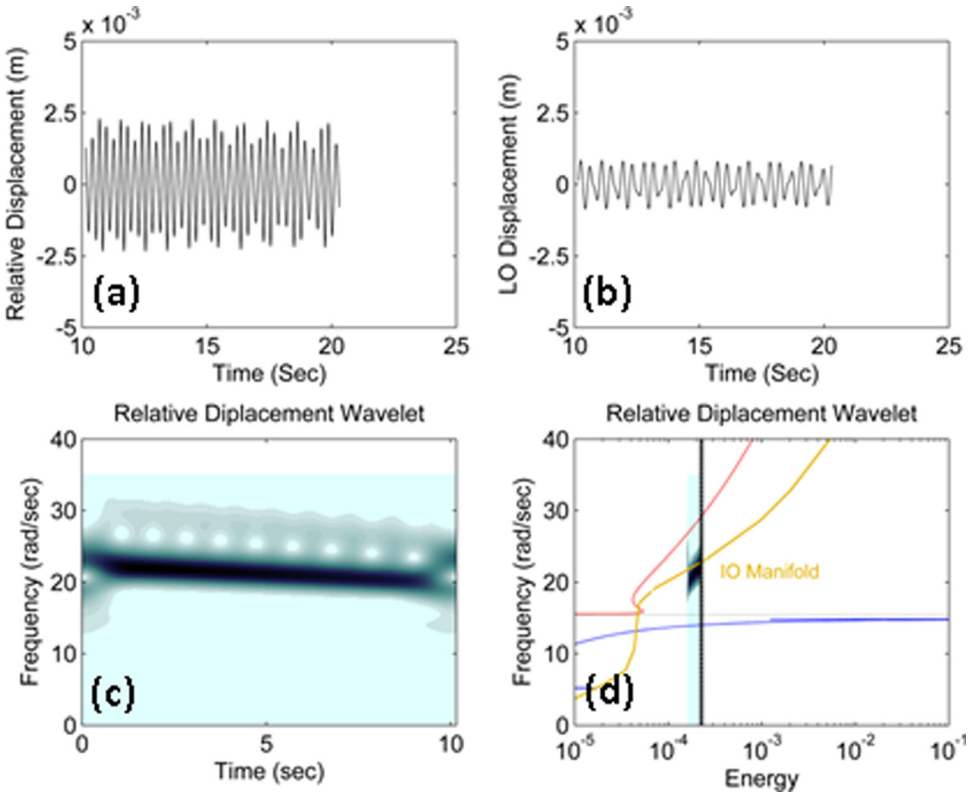

Fig. 8 Second cycle of the damped response of Fig. 6, following the second impulse: (*a*) relative displacement between the nonlinear attachment and the linear oscillator, (*b*) displacement of the linear oscillator, (*c*) wavelet spectrum of the relative displacement, and (*d*) wavelet spectrum of (*c*) on the Hamiltonian FEP

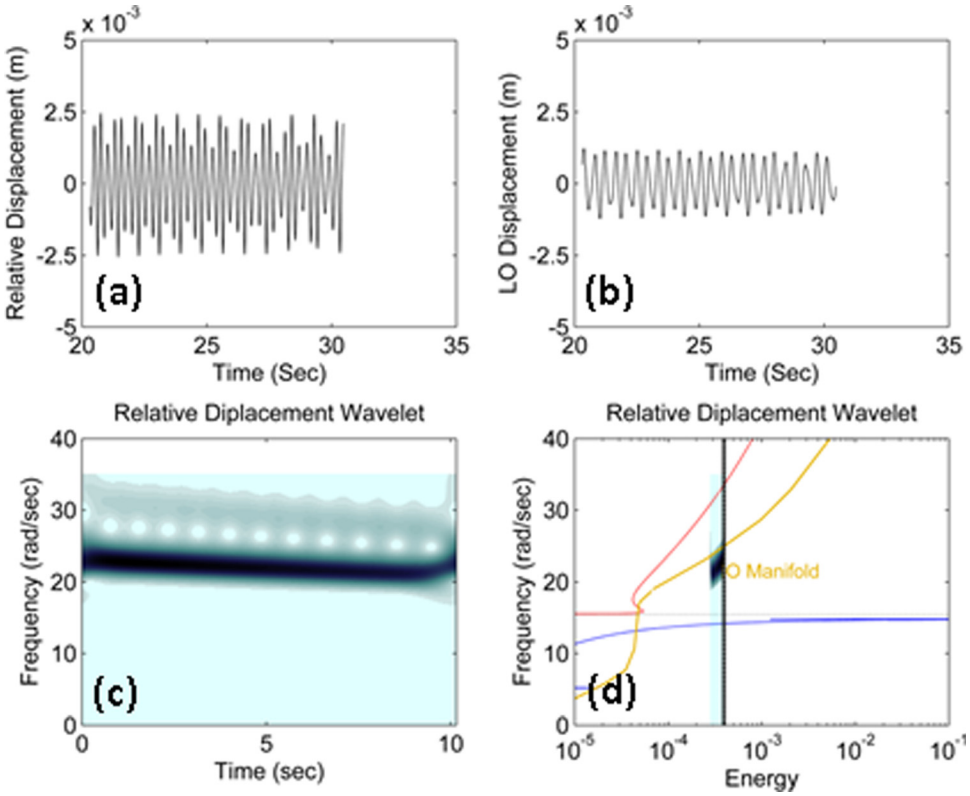

Fig. 9 Third cycle of the damped response of Fig. 6, following the third impulse: (*a*) relative displacement between the nonlinear attachment and the linear oscillator, (*b*) displacement of the linear oscillator, (*c*) wavelet spectrum of the relative displacement, and (*d*) wavelet spectrum of (*c*) on the Hamiltonian FEP

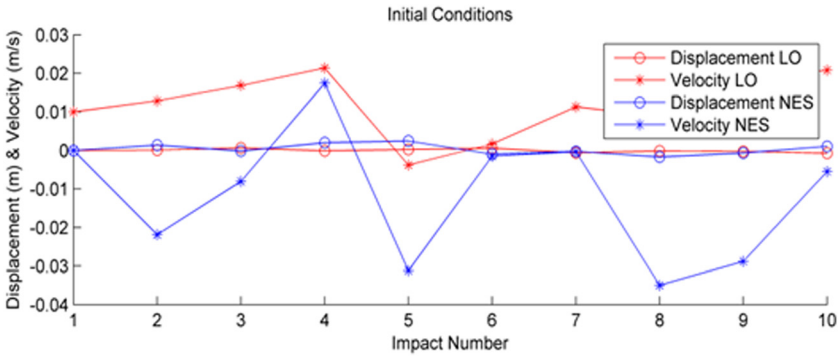

Fig. 10 Initial conditions of the linear oscillator and the nonlinear attachment at the beginning of each of the ten impulsive cycles of the damped response depicted in Fig. 6

portion of the IOM. In the previous study by Anderson [13], a similar dynamical instability was reported but this was associated exclusively with *low-frequency* IOM tracking; in that work, no high-frequency IOM tracking could be realized due to the relatively large value of the normalized mass ratio (which was close to 40% compared to the 8% value used in the present study).

The response of the system for the relatively high impulse intensity $I_0 = 0.070$ m/s is shown in Fig. 5. In this case, the high-frequency IOM tracking is more clearly visible, confirming the occurrence of high-frequency dynamic instability in this system. The high-frequency IOM tracking is evident when one considers the slowly varying strong high-frequency harmonic in the relative response of the wavelet spectrum of Fig. 5(*c*). Moreover, as seen from the wavelet spectrum superposition of Fig. 5(*d*), the response of the nonlinear attachment starts tracking the high-frequency portion of the IOM right from the start of the damped dynamics, with continuously decreasing frequency and energy for the duration of the simulation. This sustained high-frequency resonance scattering results in large-amplitude and strongly modulated oscillations of the nonlinear attachment and, hence, to the strong transient dynamic instability of the damped response. In this case, the linear oscillator oscillates at its own natural frequency (i.e., slower compared to the linear oscillator), concurrently with the complex dynamics of the nonlinear attachment.

In the next step of the computational study the repetitive impulse excitation scenario is considered, whereby the linear oscillator is forced by a periodic series of identical impulses with the system being initially at rest, as outlined by the conditions (2) and (3). The principal aim of the study is to demonstrate that it is possible to consistently bring the nonlinear attachment into a state of dynamic instability by repeatedly tracking the high-frequency portion of the IOM, as in the previous case of single impulse excitation. For consistency, the system parameters for the following computational study remain the same as in the previous single impulse excitation scenario. The damped responses of system (1), subject to the initial conditions (2) and intermediate conditions (3), were considered for a range of applied normalized impulse intensities I_0 applied at time instants $= pT$, $p = 0, 1, 2, \ldots$. Following each applied impulse the initial conditions and the energy of the system were considered, and the resulting damped transitions were studied by superimposing their wavelet spectra on the Hamiltonian frequency-energy plot (as in the previous case of single impulse excitation).

Figure 6 presents the damped response of the system for 10 applied impulses of normalized intensity $I_0 = 0.010$ m/s and normalized period $n = T/T_0 = 25$ (i.e., the period of the applied periodic impulse excitation was 25 times the natural period of oscillation of the linear oscillator). Here, note that similar to the previous case, the response of the (unexcited) nonlinear attachment is larger than the response of the (directly excited) linear oscillator, indicating the repetitive excitation of dynamic instability in this case. Moreover, the excitation of the dynamic instability after application of each impulse occurs for nonzero initial conditions of the system (in contrast to the single impulse excitation scenario), providing a first indication of robustness of the dynamic instability mechanism.

To study the damped dynamics of the system and prove the excitation of high-frequency dynamic instability after the application of the initial impulses, Figs. 7–9 present a detailed analysis of the dynamics following each of the first three impulses of Fig. 6. The level of normalized impulse intensity is chosen so that the initial energy level in the system is the same as the initial energy level of the simulation of Fig. 4, where high-frequency dynamic instability in the response of the nonlinear attachment resulted from tracking by the damped dynamics of the high-frequency portion of the IOM. The normalized impulsive period $n = 25$ was chosen according to the forcing scheme that was physically realizable in the experimental realization of the repetitive impulse scenario, as discussed in Sec. 5.

As seen in the relative displacement time series in Fig. 6, large amplitude oscillations are maintained for the duration of the simulation and for each of the impulses. Considering in detail the first cycle of the response presented in Fig. 7, the wavelet spectrum superposition on the FEP indicates that the instantaneous frequency of the nonlinear attachment is fluctuating between several of the superharmonic resonance branches existing in the neighborhood of the IOM (which are not depicted in the FEP for this system). The relative displacement time series indicates that this is a pulsing (beating) phenomenon attributed to superharmonic resonance captures (RCs), similar to that depicted in Fig. 4. Recall at this point that that damped transitions in the neighborhood of the high-frequency portion of the IOM are characterized by continuously decreasing frequency and energy in the wavelet spectrum of the corresponding time series which, clearly, is not the trend in the response of the first cycle of Fig. 7. However, considering in detail the following cycle depicted in Fig. 8, the wavelet spectra superposition on the FEP indicate that the damped response of the relative response of the nonlinear attachment is now tracking the high-frequency portion of the IOM for the entire duration of the second cycle (i.e., the response of the system between the second and the third impulses). This state of sustained resonance scattering (SRS) results in the relatively high energy transfer from the linear oscillator to the nonlinear attachment, as depicted by the high amplitude oscillations in the relative displacement time series and the resulting high-frequency dynamic instability.

In addition, by examining the third cycle of the damped response depicted in Fig. 9 in detail, it is deduced that the wavelet spectrum of the relative response between the nonlinear attachment and the linear oscillator again tracks the high-frequency portion of the IOM for the entire duration of this cycle. In fact, the response of the system during the third cycle is similar to the response during the second cycle, despite the different initial

Table 3 Summary of resonance captures for the repeated impulse excitation scenario with $I_0 = 0.010$ m/s and $n = 25$

Impulse number	Type of dynamic response
1	Superharmonic RC
2	SRS
3	SRS
4	SRS
5	SRS
6	SRS (primarily)
7	Superharmonic RC
8	SRS
9	SRS
10	SRS

conditions of the system at the start of each cycle (as shown in Fig. 10). This indicates that the described high-frequency instability can be robustly excited, even for varying initial conditions of the system at the beginning of each cycle following repetitive impulse excitation.

The robustness of the excitation of high-frequency dynamic instability in this case is further confirmed by the results reported in Table 3, where a summary of the analysis of the dynamic responses for all ten cycles of the damped response of Fig. 6 is provided. Two different types of damped dynamics can be realized in this case, namely, superharmonic resonance capture (RC) (similar to the response of the first cycle in Fig. 7) and sustained resonance scattering (SRS) (similar to the responses of the second and the third cycles in Figs. 8 and 9); eight of the ten impulsive cycles correspond to high-frequency dynamic instability of the response of the nonlinear attachment, tracking the high-frequency IOM. More specifically, as seen in the relative displacement time series of Fig. 6, impulsive responses of the first and seventh cycles exhibit similar qualitative features, exhibiting the superharmonic frequency fluctuations. It is interesting to note that the dynamics during the sixth impulsive cycle escapes the SRS near the end of the cycle; this might explain why the dynamics in the seventh cycle exhibits superharmonic resonance capture. However, following this, the dynamics of the eighth cycle returns to a state of SRS and the high-frequency dynamic instability is excited again. This repeated excitation of the SRS occurs despite the different initial conditions of the system at the beginning of each cycle following an impulse excitation as depicted in Fig. 10. An interesting observation is that the SRS (and high-frequency dynamic instability) appears to occur for impulsive cycles where the nonlinear attachment has an initial velocity magnitude greater than a certain threshold; i.e., $\dot{v}|(pT+)| > 0.005$ m/s. Further analytical verification of this observation will be the scope of future work.

Motivated by the previous numerical results and the theoretically predicted robust excitation of high-frequency dynamic instability of the system under single and repeated impulsive forcing, an experimental study was undertaken in order to confirm the theoretical predictions. The results of this study are discussed in Sec. 5.

5 Experimental Study

The fixture is presented in Fig. 11. The experimental system consists of two masses that oscillate along an air track, which greatly reduces damping due to friction. The more massive linear oscillator is grounded through a linear leaf spring, while the lighter nonlinear attachment is coupled to the linear oscillator using a piano wire of diameter equal to 0.5 mm. The strong stiffness nonlinearity required for the realization of the high-frequency dynamic instability is implemented by means of the piano wire oriented to be perpendicular to the direction of the motion of the attachment; when this wire has no pretension, its transverse deformation gives rise to an essential stiffness nonlinearity whose dominant component is third order (i.e., pure cubic

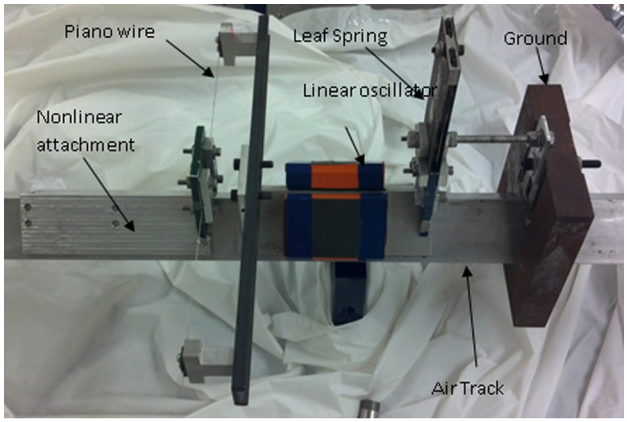

(a)

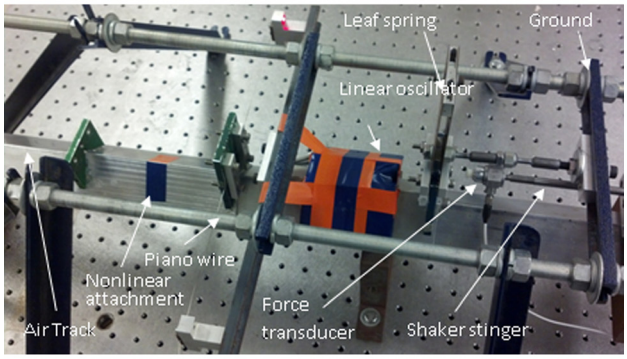

(b)

Fig. 11 Experimental realization of the system of Fig. 1: configuration for (*a*) single impulse excitation, and (*b*) periodic impulse excitation

nonlinearity [12]). Although the piano wire is mounted so that there is no pretension in the wire in order to minimize any linear component in the coupling stiffness of the nonlinear attachment, nevertheless, a small linear term occurs, as discussed in the following text; however, as pointed out in Ref. [12] this small linear term is not expected to affect the strongly nonlinear dynamical phenomena that need to be validated by the experimental study. Moreover, an additional small linear term in the coupling stiffness is inevitable due to the force that the air track imparts on the nonlinear attachment. The air track pressure is set to a near minimum value of 50 psi to support the weight of the linear oscillator and this pressure adds an artificial linear component to the coupling stiffness due to the lightweight nature of the nonlinear attachment.

Single impulsive forces are applied to the linear oscillator by means of an impact hammer, whereas periodic impulsive forces are applied by means of a long-stroke shaker. The parameter values of the experimental system were identified by performing linear modal analysis (for the parameters of the linear oscillator) and nonlinear system identification utilizing the restoring force surface

Table 4 Experimentally identified system parameters

Parameter	Value
m_1	1.9853 Kg
m_2	0.1750 Kg
k_1	469 N/m
k_3	$8.568 \times 10^{\alpha}$ N/m$^{\alpha}$
α	2.95
k_{lin}	80.0 N/m
b_1	0.0726 N s/m
b_2	0.0200 N s/m

method [18,19] (for the nonlinear attachment). The system parameters were identified, as shown in Table 4. Note that the experimentally identified exponent of the essential stiffness nonlinearity is $\alpha = 2.95$ which, although close, is not exactly equal to the theoretically assumed cubic nonlinearity used in the theoretical study of Sec. 4. Moreover, in the experimental system a small but nonnegligible linear stiffness component for the nonlinear (coupling) stiffness of the attachment equal to $k_{\text{lin}} = 80$ N/m is identified, which again is contrary to the assumption of pure nonlinearizable stiffness nonlinearity of the attachment in the theoretical model of Sec. 4. As discussed in Ref. [12], however, this small linear component is not expected to affect the dynamics in a significant way. It is noteworthy that damping in the experimental system is rather weak; the numerical study confirms the assumption that weak viscous damping is essential for obtaining the high-frequency dynamical instability, thus the experimental model satisfies this requirement. It is important to note that some uncertainty existed in the identified system parameters due to the effect of the air track pressure on the carts, unmodeled friction effects in the system, and occasional contact of the carts with the air track. All Hamiltonian frequency-energy plots depicted in this section are identical to the one depicted in Fig. 2; i.e., they are based on the preceding experimentally identified system parameters but for the exponent of the nonlinearity which was adjusted to 3 (i.e., exact cubic nonlinearity was assumed instead of the experimental exponent value of 2.95), and the linear component of the stiffness nonlinearity which was omitted (i.e., it was assumed to be $k_{\text{lin}} = 0$). This provides a measure of consistency in the interpretation of the experimental responses when their wavelet spectra are depicted in the underlying Hamiltonian FEP.

As in the computational study of Sec 4, first the single impulse excitation scenario is considered. The computational study predicted the impulsive excitation levels that would allow for sustained resonance scattering in the higher frequency portion of the IOM (PCB Piezotronics, Inc., Depew, NY). As stated earlier, for the single impulse excitation a PCB modal hammer was used to apply the excitation to the linear oscillator with the system initially at rest. The velocity time series measurements of the two oscillators were obtained using two Polytec VibraScan laser vibrometers at a sampling frequency of 512 Hz. The data acquisition for the two systems was synchronized using the impact hammer as the triggering mechanism, with a small pretrigger time of 640 ms. The synchronized response of the oscillator system was very important for the accurate computation of the wavelet spectra of the relative displacement time series and the relative displacement frequency-energy plots, since it eliminated any phase-lags between the measured responses of the linear oscillator and the nonlinear attachment. The raw velocity time series data were then numerically integrated once to obtain the corresponding displacement time series for each of the two oscillating components of the system. The displacement time series data were corrected using a high pass 4th order Butterworth filter with a cutoff frequency of 1.28 Hz to eliminate drift in the data from the signal noise. The instantaneous total system energy during the dynamics could then be computed similarly to the numerical case, followed by numerical computation of the wavelet spectra of the relative displacement time series and superposition of these wavelet spectra on the Hamiltonian FEP, exactly as in the computational study.

The system was forced using a wide range of excitation magnitudes corresponding to situations in which sustained resonance scattering was numerically observed. Exciting a damped transition on the lower frequency portion of the IOM for this system proved to be unobtainable (contrary to Ref. [13], where a heavier nonlinear attachment was used and low-frequency IOM tracking was the only possibility). Following the notation of Sec. 4 the predicted range for a transition on the lower portion of the IOM (as in the transition of Fig. 3) was for an initial normalized impulsive intensity I_0 in the range $0.007 - 0.012$ m/s. In practical terms, this impulse range was hard to excite using a modal hammer, since physical hammer excitations less than $I_0 = 0.015$ m/s caused very low amplitude oscillations, as predicted by the numerical investigation. However, in the experimental tests these low amplitude oscillations were predominantly linear, indicating that the air track pressure was having a stronger polluting effect on the dynamics of the lightweight nonlinear attachment at these low amplitudes. Therefore, the remaining experiments focused on exciting the

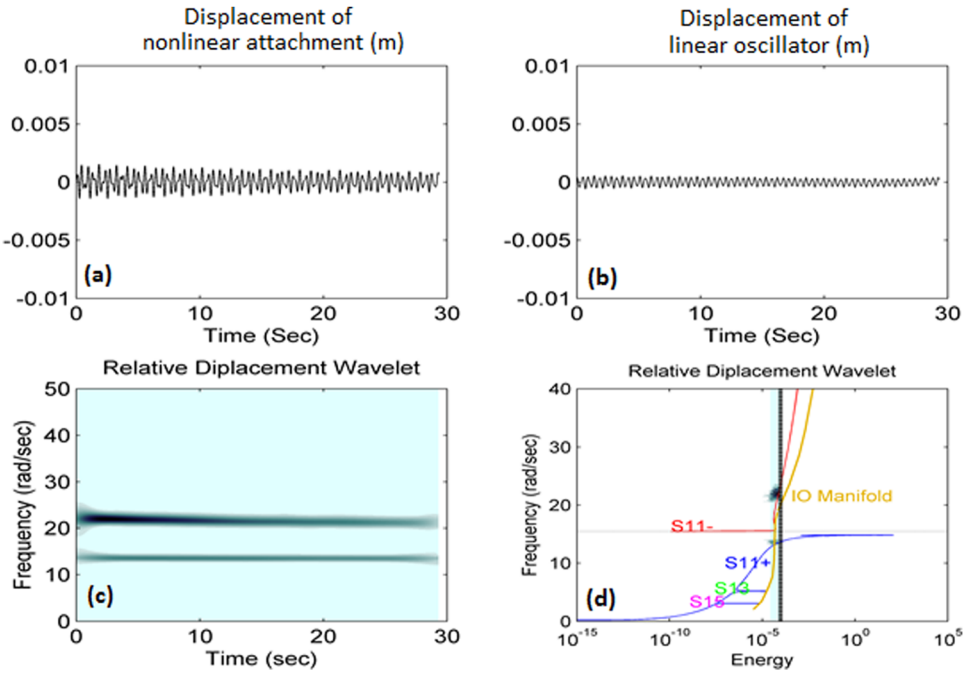

Fig. 12 Damped experimental response for the single impulse excitation of normalized intensity $I_0 = 0.0198$ m/s: (*a*) displacement of the nonlinear attachment, (*b*) displacement of the linear oscillator, (*c*) wavelet spectrum of the relative displacement, and (*d*) wavelet spectrum of (*c*) superimposed on the Hamiltonian FEP

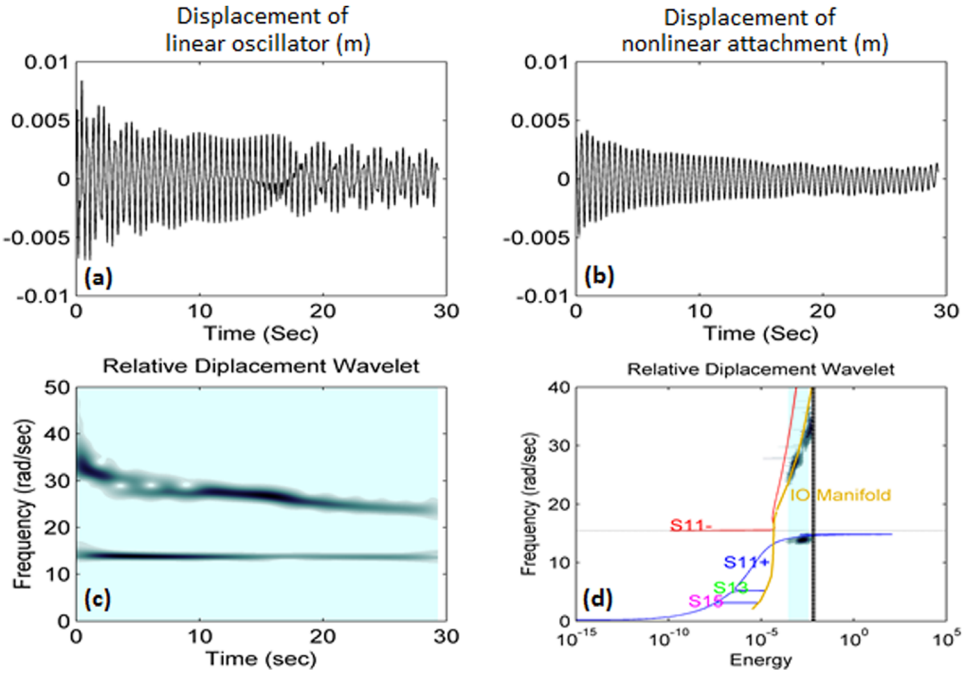

Fig. 13 Damped experimental response for single impulse excitation of normalized intensity $I_0 = 0.1454$ m/s: (*a*) displacement of the nonlinear attachment, (*b*) displacement of the linear oscillator, (*c*) wavelet spectrum of the relative displacement, and (*d*) wavelet spectrum of (*c*) superimposed on the Hamiltonian FEP

upper portion of the IOM,where the theoretically predicted high-frequency dynamical instability was expected to occur.

The predicted range for a transition on the upper portion of the IOM (as in the transitions of Figs. 4 and 5) was for normalized impulse intensities of $0.014\,\text{m/s} < I_0 < 0.080\,\text{m/s}$. In practical terms this impulsive magnitude range corresponded to an energy range 10^{-4}–10^{-2} J of the FEP depicted in Fig. 2. In the experimental tests this energy range was robustly excitable with the modal hammer, with the resulting high-amplitude oscillations of the system exhibiting strongly nonlinear characteristics, indicating that the air track had a negligible (linear) effect on the dynamics. It is important to note here that the numerically predicted impulse magnitudes did not correspond directly to the required physical impulse magnitudes to obtain transitions in the same energy range. This was because the forcing in the numerical simulation was in the form of a Dirac delta function, while the forcing practically realized by the modal hammer was approximately in the form of a half-sine wave. This, however, did not present a problem in the experimental forcing scheme, but rather provided an important distinction between the numerical simulation and experimental trial.

The experimental response of the system of Fig. 11(*a*) for a normalized impulse intensity equal to $I_0 = 0.0198$ m/s is depicted in Fig. 12. This initial excitation energy input into the linear oscillator achieved by means of the modal hammer is comparable to the energy input depicted in the theoretical response of Fig. 4. Indeed, the responses and the wavelet spectra of the responses of the linear and nonlinear oscillators compare favorably. Similar to the theoretical case of Fig. 4, the dynamics of the nonlinear attachment occurs in the neighborhood of the intersection between the out-of-phase backbone branch $S11-$ and the high-frequency portion of the IOM for the entire duration of the simulation. That this is, indeed, the case is verified by the nearly constant wavelet spectrum of the relative response in Fig. 12(*c*). This result is typical for the experimental setup with initial excitation levels of $\sim 10^{-4.3}$ J and below. As stated earlier, damped transitions of the dynamics in the neighborhood of the lower frequency part of the IOM could not be experimentally realized with the current experimental setup.

A different picture of the damped dynamics is obtained for stronger applied impulses. Figure 13 depicts the experimental response of the system for a higher normalized impulse intensity equal to $I_0 = 0.1454$ m/s. This initial excitation energy input into the linear oscillator by means of the modal hammer is comparable to the energy input in the theoretical computation depicted in Fig. 5. Similar to the theoretical result, the experimental responses of Fig. 13 verify the occurrence of high-frequency dynamical instability resulting by tracking the higher frequency portion of the IOM. That this is, indeed, the case is verified by the slowly (and continuously) decreasing frequency spectrum of the relative response of Fig. 13(*c*). Hence, the theoretical prediction of high-frequency dynamical instability of Sec. 4 is experimentally validated. As seen in the superposition of the wavelet spectrum of the relative response on the Hamiltonian FEP of Fig. 13(*d*), the nonlinear dynamics starts tracking the high-frequency portion of the IOM right from the beginning of the motion and keeps on tracking the IOM with decreasing frequency and energy (due to damping dissipation). Interesting dynamics then occur at $t = 3$ s, when the instantaneous frequency of the relative oscillation starts fluctuating between different resonances in the neighborhood of the upper IOM and the $S11+$ backbone branch. Following this phase of the dynamics, the damped dynamics again starts tracking the upper portion of the IOM at $t = 10$ s and for the remainder of the presented window of experimental measurement. The tracking of the higher frequency portion of the IOM results in high-frequency dynamic instability of the system in the form of 'bursts' in the velocity time series of the nonlinear attachment (see Fig. 13(*b*)).

The experimental study indicates that this state of sustained resonance scattering by tracking the upper portion of the IOM and the ensuing instability in the response of the nonlinear attachment is robust (and fully reproducible) for normalized impulse intensities in the range of $10^{-4}\,\text{J} < I_0 < 10^{-2}\,\text{J}$. In fact, high-frequency dynamic instability due to tracking of the upper portion of the IOM was observed in 17 out of 20 experimental trials performed in the aforementioned energy range, indicating that the reported dynamic instability is robust in the experimental system.

In an additional series of experiments, the periodic impulsive excitation scenario is considered using the modified experimental

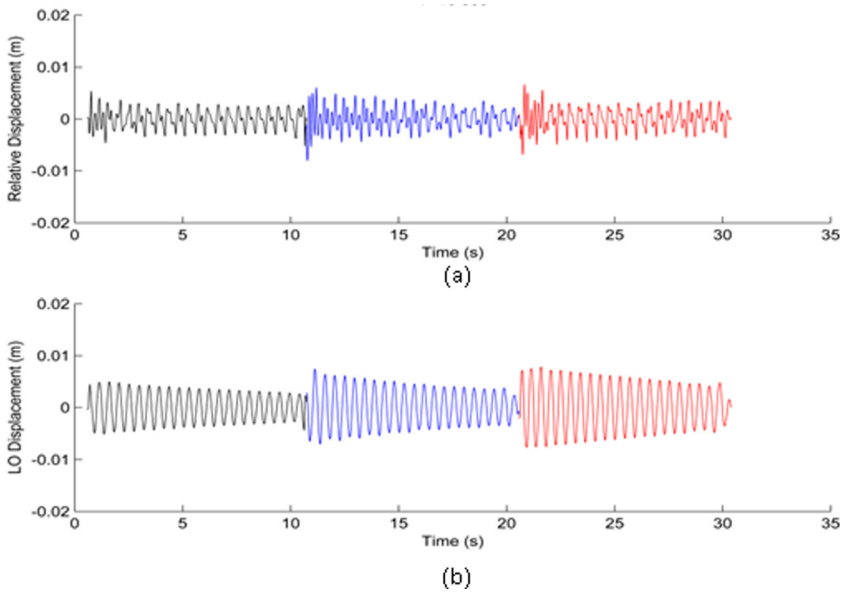

Fig. 14 Experimental damped response for periodic impulse excitation of normalized intensities $I_0 = 0.2262$ m/s (first cycle), $I_0 = 0.3806$ m/s (second cycle), and $I_0 = 0.2829$ m/s (third cycle): (*a*) relative displacement between the nonlinear attachment and the linear oscillator, and (*b*) displacement of the linear oscillator

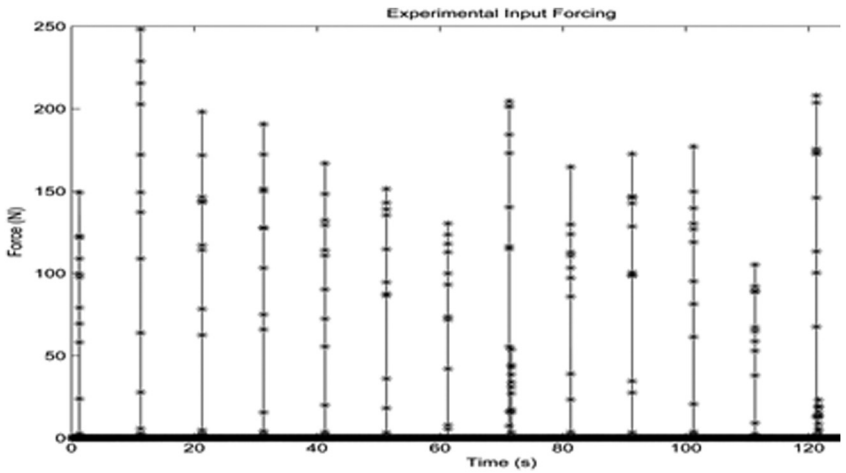

Fig. 15 Experimentally realized impulsive forces for the experimental test

fixture of Fig. 11(*b*) which enabled the excitation of the linear oscillator by a periodic series of identical impacts. As seen in Fig. 11(*b*) the core experimental fixture remains the same as the experimental fixture depicted in Fig. 11(*a*) for the single impulse excitation scenario; however, in the present case the ground for the linear oscillator was shifted to a separately standing structure that surrounds the air track. An APS Dynamics ELECTRO-SEIS® Model 400 long-stroke electromagnetic shaker was aligned along the axial direction of the air track to the right of the linear oscillator, with respect to Fig. 11(*b*). The shaker stinger was supported by a self-aligning linear ball bearing and aligned with a suitable impact location in line with the vertical and horizontal axial center of mass of the linear oscillator. A PCB force transducer with a hard plastic tip (as was the case with the modal hammer) was mounted to the tip of the stinger in order to measure the precise waveform of the applied impulsive force that was applied during each cycle. Elastic bands within the shaker were adjusted so that the separation between the linear oscillator and stinger tip was held at 0.5 in. prior to the application of each impulse. A positive half-square waveform of duration less than 25 ms was input to the shaker controller followed by a negative half-square waveform of duration 100 ms. The positive square wave applied a fast impulsive force to the linear oscillator similar to the impulse imparted by the modal hammer in the single impulse excitation scenario. The negative square wave quickly retracted the shaker armature and stinger in order to avoid undesirable double impulse excitations to the linear oscillator. The elastic bands then brought the stinger back to the prescribed 0.5 in. separation before the next impulse was applied by the shaker. This waveform was then applied to the system at the desired impact period and at the desired impulsive magnitude. For the experiments, a period equal to $T \sim 10$ s per impulse was selected in order to match the normalized period $n = 25$ used in the previous computational study for this excitation scenario.

The velocity time series measurements for the two oscillators were obtained using the two Polytec laser vibrometers, but at a higher sampling frequency of 1024 Hz in order to obtain more accurate forcing data. Due to the sample size restrictions of the Polytec scanning system in use, the duration of the experiment was limited to ~ 30 s or three impulse cycles. Moreover, the force

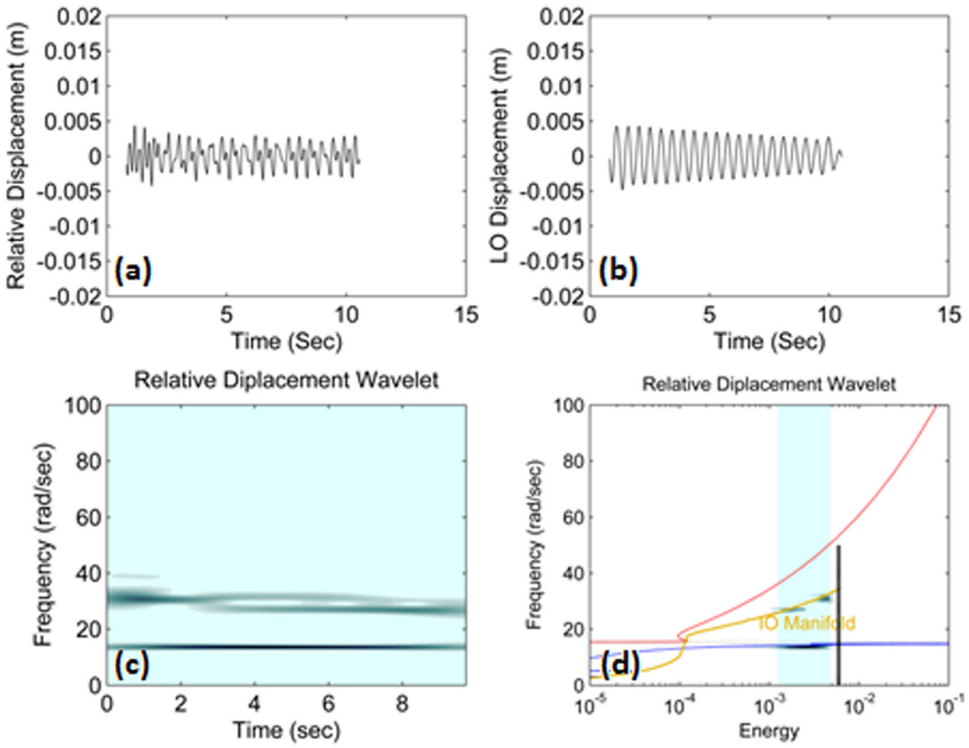

Fig. 16 First cycle of the damped response of Fig. 14, following the first impulse: (*a*) relative displacement between the nonlinear attachment and the linear oscillator, (*b*) displacement of the linear oscillator, (*c*) wavelet spectrum of relative the displacement, and (*d*) wavelet spectrum of (*c*) on the Hamiltonian FEP

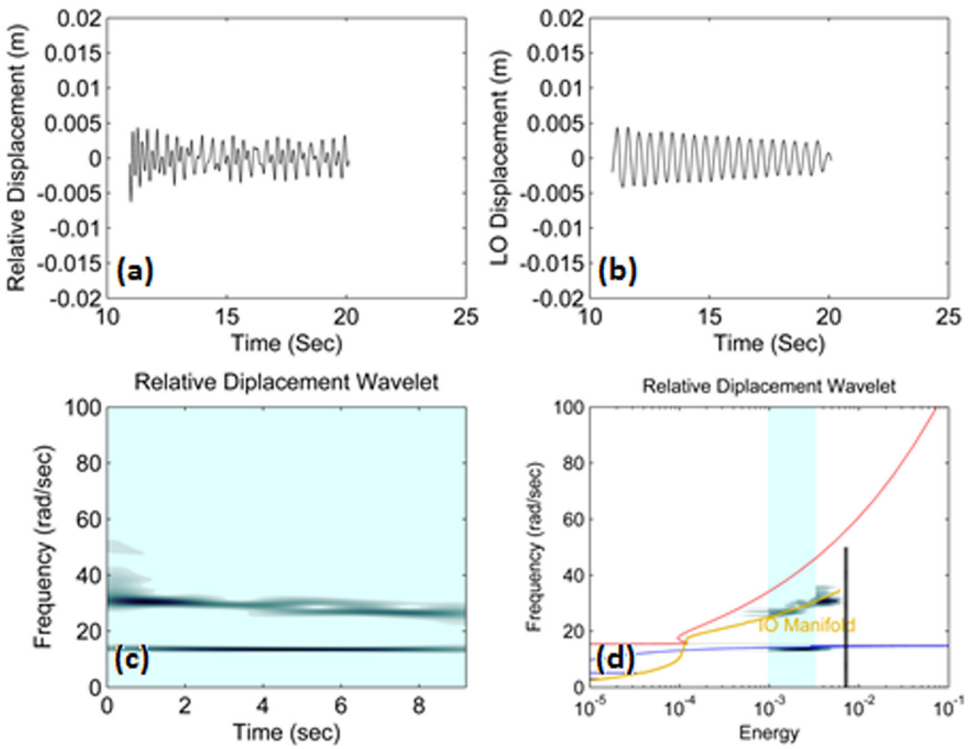

Fig. 17 Second cycle of the damped response of Fig. 14, following the second impulse: (*a*) relative displacement between the nonlinear attachment and the linear oscillator, (*b*) displacement of the linear oscillator, (*c*) wavelet spectrum of the relative displacement, and (*d*) wavelet spectrum of (*c*) on the Hamiltonian FEP

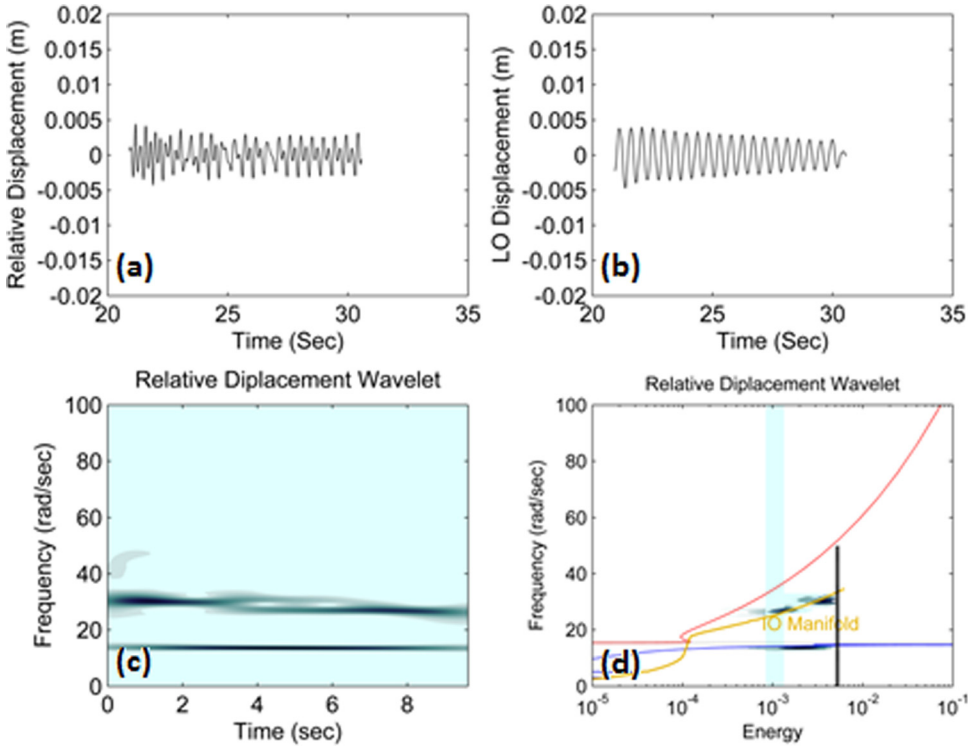

Fig. 18 Third cycle of the damped response of Fig. 14, following the third impulse: (*a*) relative displacement between the nonlinear attachment and the linear oscillator, (*b*) displacement of the linear oscillator, (*c*) wavelet spectrum of the relative displacement, and (*d*) wavelet spectrum of (*c*) on the Hamiltonian FEP

transducer at the tip of the striker was used to synchronize (trigger) the data acquisition for the two laser systems, with a small pretrigger time of 640 ms. The data was processed the same way as for the previously described single impulse experimental trials. The forcing data from the force transducer was used to split the entire experimental trial into impulsive cycles, allowing for separate FEP analysis of the transient dynamics of the system at each cycle. As in the case of the single impulse experimental trials, only the cases where damped transitions occurred on the upper branch IOM triggering dynamic instability will be presented here.

As described by the conditions (3), the two oscillators have a nonzero state of motion before the application of the pth impulse, which differentiates the dynamics from the case of single impulse excitation. It follows that the initial energy in the system is now a function of the displacement and velocity of the two oscillators at the application of each repetitive impulse, rather than just the velocity of the linear oscillator as in the previous case of a single impulse. Nevertheless, the computational study of the previous Sec. 4 predicted that sustained resonance scattering (and, hence, high-frequency dynamic instability in the response of the nonlinear attachment) could be robustly realized in this case, especially if the nonlinear attachment possesses a relatively high initial energy at the beginning of each impulsive cycle.

Figure 14 depicts the experimental responses for the first three impulsive cycles of the system. The impulse intensities were chosen so that the initial energy levels of the system were in the range of $10^{-4} - 10^{-2}$ J, in which the previous theoretical study predicted the occurrence of high-frequency dynamical instability resulting from repeated tracking of the higher frequency portion of the IOM. As stated earlier, data was acquired only for three impulsive cycles due to hardware restrictions. As seen in the relative displacement time series of Fig. 14(*a*), the nonlinear attachment undergoes high-frequency complex oscillations which occur in the nonlinear attachment. Here, note that this is different than the computational results depicted in Fig. 6 where the amplitudes of oscillation of the nonlinear attachment were larger than those of the linear oscillator. This can be attributed to the fact that the forcing scheme was slightly different in the experimental case. In particular, due to the finite forcing waveform that could be practically realized by the shaker, each impulse delivered to the linear oscillator was of finite duration (in contrast to the δ-function excitation in the theoretical case), of slightly varying intensity, and at slightly varying time periods between impulses. The exact forcing scheme realized in this particular experimental trial is shown in Fig. 15 and confirms these assertions regarding the uncertainties in the repetitive series of impulsive excitations.

The first three impulsive cycles of the experimental response of Fig. 14 were analyzed in detail as in the theoretical case and the results are depicted in Figs. 16–18. As seen from the experimental impulsive forces depicted in Fig. 15, the forces applied to the linear oscillator are not of the same magnitude and are only nearly periodic. Focusing on the results of Fig. 16(*d*), it is noted that the wavelet spectra-FEP superposition does not clearly show the frequency transition on the upper portion of the IOM for the relative displacement; however, the wavelet spectrum of the relative displacement depicted in Fig. 16(*c*) indicates that the dynamics of the nonlinear attachment briefly tracks the IOM, but primarily gets captured on the high-frequency superharmonic resonance branches. The instantaneous frequency of the nonlinear attachment then fluctuates between two superharmonic resonance branches, in similarity to the numerical simulation presented in Fig. 7, which depicts the first cycle of the theoretical case.

Considering the second impulsive cycle of Fig. 17, the results clearly indicate the capture of the dynamics on the upper portion of the IOM right from the beginning of the cycle. This experimentally confirms the theoretical prediction and shows that the high-frequency dynamical instability can be robustly excited, even by repetitive impulsive forcing with the previously mentioned uncertainties. It is noteworthy that interesting dynamics occur at $t = 4$ s

within the second impulsive cycle, when the frequency starts fluctuating between different resonances in the neighborhood of the upper IOM. After this intermediate dynamics, the nonlinear attachment returns to tracking the upper IOM at $t = 6.5$ s for the remainder of the cycle.

The third impulsive cycle is considered in Fig. 18 and indicates similar behavior to the second cycle, with consistent excitation of the high-frequency dynamical instability associated with tracking by the dynamics of the upper portion of the IOM. This further confirms the capacity of the strongly nonlinear attachment to engage in sustained resonance scattering on the IOM in the second impulsive excitation scenario. An additional series of experimental tests similar to the one presented in Figs. 16–18 were performed. The high-frequency dynamical instability was readily repeatable, indicating that sustained resonance scattering is robust in the impulsively forced system.

6 Concluding Remarks

This report presented a computational and experimental study of the impulsive dynamics of a linear oscillator coupled to a lightweight attachment by means of an essentially nonlinear stiffness nonlinearity of the third degree. The term 'essential nonlinearity' describes the lack of (or the presence of a small) linear component in the stiffness characteristic. This strong nonlinearity is realized by geometric effects, i.e., by introducing nonlinear effects appearing due to midplane stretching of a linearly elastic wire with negligible or very small internal tension. The presence of essential stiffness nonlinearity leads to a negligible (or very small) linearized eigenfrequency of the attachment; in effect, removing any preferential resonance frequency in its dynamics. This enables it to engage in nonlinear resonance with the linear oscillator over broad frequency and energy ranges. The resulting broadband dynamics of the strongly nonlinear attachment is manifested in the form of high-frequency dynamical instabilities, whereby the nonlinear attachment reacts to impulsive excitation of the linear oscillator with relatively high-amplitude oscillations of varying frequency content.

These high-frequency oscillations of the attachment are due to the continuous resonance scattering of its dynamics on the high-frequency portion of the impulsive orbit manifold (IOM) of the system, a dynamical phenomenon that is exclusively due to the essential stiffness nonlinearity of the problem and cannot exist in linear or weakly nonlinear settings. As a result, this system represents a good candidate for vibration energy harvesting in situations where a primary system is forced by single or repetitive impulses; lightweight attachments of the type considered in this work can be designed so that the resulting high-frequency dynamical instabilities can be employed for energy harvesting. The aim of the current work of the authors is in the development of such harvesting devices.

Acknowledgment

This work was supported in part by the National Science Foundation Grant No. CMMI-1100722.

References

[1] Gendelman, O., Vakakis, A. F., Bergman, L. A., and McFarland, D. M., 2010, "Asymptotic Analysis of Passive Nonlinear Suppression of Aeroelastic Instabilities of a Rigid Wing in Subsonic Flow," SIAM J. Appl. Math., **70**(5), pp. 1655–1677.

[2] Lee, Y. S., Kerschen, G., Vakakis, A. F., Panagopoulos, P., Bergman, L. A., and McFarland, D. M., 2005, "Complicated Dynamics of a Linear Oscillator With a Light, Essentially Nonlinear Attachment," Physica D, **204**, pp. 41–69.

[3] Andersen, D., Vakakis, A. F., Starosvetsky, Y., and Bergman, L., 2012, "Dynamic Instabilities in Coupled Oscillators Induced by Geometrically Nonlinear Damping," Nonlinear Dyn., **67**, pp. 807–827.

[4] Den Hartog, J. P., 1956, *Mechanical Vibrations*, McGraw-Hill, New York.

[5] Vakakis, A. F., 2001, "Inducing Passive Nonlinear Energy Sinks in Linear Vibrating Systems," ASME J. Vibr. Acoust., **123**(3), pp. 324–332.

[6] Vakakis, A. F., Manevitch, L. I., Gendelman, O., and Bergman, L. A., 2003, "Dynamics of Linear Discrete Systems Connected to Local Essentially Nonlinear Attachments," J. Sound Vib., **264**, pp. 559–577.

[7] Kerschen, G., Lee, Y., Vakakis, A. F., McFarland, D. M., and Bergman, L. A., 2006, "Irreversible Passive Energy Transfer in Coupled Oscillators With Essential Nonlinearity," SIAM J. Applied Math., **66**(2), pp. 648–679.

[8] Gendelman, O., Gorlov, D., Manevitch, L. I., and Musienko, A., 2005, "Dynamics of Coupled Linear and Essentially Nonlinear Oscillators With Substantially Different Masses," J. Sound Vibr., **286**, pp. 1–19.

[9] Lee, Y. S., Nucera, F., Vakakis, A. F., McFarland, D. M., and Bergman, L. A., 2009, "Periodic Orbits, Damped Transitions and Targeted Energy Transfers in Oscillators With Vibro-Impact Attachments," Physica D, **238**, pp. 1868–1896.

[10] Gendelman, O. V., 2001, "Transition of Energy to Nonlinear Localized Mode in Highly Asymmetric System of Nonlinear Oscillators," Nonlinear Dyn., **25**, pp. 237–253.

[11] Gourdon, E., Alexander, N. A., Taylor, C. A., Lamarque, C. H., and Pernot, S., 2007, "Nonlinear Energy Pumping Under Transient Forcing With Strongly Nonlinear Coupling: Theoretical and Experimental Results," J. Sound Vib., **300**, pp. 522–551.

[12] Vakakis, A. F., Gendelman, O., Bergman, L. A., McFarland, D. M., Kerschen, G., and Lee, Y. S., 2008, *Nonlinear Targeted Energy Transfer in Mechanical and Structural Systems*, Springer-Verlag, New York.

[13] Anderson, D., Starosvetsky, Y., Mane, M., Hubbard, S., Remick, K., Wang, X., Vakakis, A., and Bergman, L., 2012, "Non-Resonant Damped Transitions Resembling Continuous Resonance Scattering in Coupled Oscillators With Essential Nonlinearities," Physica D, **241**, pp. 964–974.

[14] Itin, A. P., Neishtadt, A. I., and Vasiliev, A. A., 2000, "Captures Into Resonance and Scattering on Resonance in Dynamics of a Charged Relativistic Particle in Magnetic Field and Electrostatic Wave," Physica D, **141**, pp. 281–296.

[15] Neishtadt, A. I., 2006, "Scattering by Resonances," Celest. Mech. Dyn. Astron., **65**(1-2), pp. 1–20.

[16] Vainchtein, D. L., Neishtadt, A. I., and Mezic, I., 2006, "On Passage Through Resonances in Volume-Preserving Systems," Chaos, **16**, p. 043123.

[17] Kerschen, G., Gendelman, O., Vakakis, A. F., Bergman, L. M., and McFarland, D. M., 2008, "Impulsive Periodic and Quasi-Periodic Orbits of Coupled Oscillators With Essential Stiffness Nonlinearity," Commun. Nonlinear Sci. Numer. Simul., **13**, pp. 959–978.

[18] Masri, S. F. and Caughey, T. K., 1979, "A Nonparametric Identification Technique for Nonlinear Dynamic Problems," ASME J. Appl. Mech., **46**, pp. 433–447.

[19] Worden, K., 1990, "Data Processing and Experiment Design for the Restoring Force Surface Method, Part I: Integration and Differentiation of Measured Time Data," Mech. Syst. Signal Process., **4**(4), pp. 295–319.